2011-05-01

Liquid Crystal infiltrated Photonic Crystal Fiber for Electric Field Intensity Measurements.

Sunish Mathews
Dublin Institute of Technology, sunish.mathews@dit.ie

Gerald Farrell
Dublin Institute of Technology, gerald.farrell@dit.ie

Yuliya Semenova
Dublin Institute of Technology, yuliya.semenova@dit.ie

Recommended Citation

Mathews, S., Farrell, G., Semenova, Y.:Liquid Crystal infiltrated Photonic Crystal Fiber for Electric Field Intensity Measurements. *Applied Optics*, Volume 50, Issue 14, 2011. doi:10.1364/AO.50.002628

Liquid crystal infiltrated photonic crystal fibers for electric field intensity measurements

Sunish Mathews*, Gerald Farrell and Yuliya Semenova

Photonics Research Centre, School of Electronic and Communications Engineering, Dublin Institute of Technology, Dublin, Ireland

*Corresponding author: sunish.mathews@dit.ie

Abstract

The application of nematic liquid crystal infiltrated photonic crystal fiber as a sensor for electric field intensity measurement is demonstrated. The device is based on an intrinsic sensing mechanism for electric fields. The sensor probe, which consists of a 1 cm infiltrated section of photonic crystal fiber with a lateral size of ~ 125 microns, is very compact with small size and weight. A simple all-fiber design for the sensor is employed in an intensity based measurement scheme. The transmitted and reflected power response of the infiltrated photonic crystal fiber is shown to have a linear response with the applied electric field. The sensor is operated in the telecommunication window at 1550 nm. The temperature dependence of the device at this operating wavelength is also experimentally studied and discussed. These structures can be used to accurately measure electric field intensity and can be used for the fabrication of all-fiber sensors for high electric field environments as both an in-line and reflective type point sensor.

OCIS Codes:

(060.2370) Fiber optics sensors; (060.5295) Photonic crystal fibers; (160.3710) Liquid crystals

1. Introduction:

Photonic crystal fibers (PCFs) have recently attracted much attention for applications in optical sensing. One very attractive feature of PCF is that dynamic modification of their guiding properties is possible by filling the micro-holes with substances whose refractive index can be tuned or influenced by external fields. Infiltration of liquid crystal (LC) materials into the micro-holes of the PCF has been extensively studied for various in-fiber tunable device applications [1-6]. Infiltration of LC materials makes the PCF susceptible to external field variations, a property which can be utilized to fabricate all-fiber sensors for parameters such as temperature, magnetic fields and electric fields.

Conventional electric field sensors use antennas, conductive electrodes or metal connections and because of their metallic content are very likely to very often perturb the unknown field. Fiber optic sensors for voltage and electric field measurement are widely used in both electromagnetic compatibility measurements and in the electric power industry. Unlike their conventional counterparts, fiber optic based electric field sensing techniques minimally disturb the electric field and apart from the sensor head, the connecting fibers are inherently immune to electromagnetic interference [7]. They have several economic and performance advantages over conventional electrode based sensors, most importantly they can provide true dielectric isolation between the sensor and the interrogation system in the presence of very high electric fields or voltages. A wide variety of fiber optic based electric field sensing schemes have been proposed and reported to date. These are mostly based on electro-optical crystals employed either in bulk optics or free-space type configurations or in an integrated waveguide type configuration [8-12]. However such schemes have a number of disadvantages such as high losses due to the presence of bulk optics, high coupling losses, costly integration with optical fiber, limited mechanical reliability and difficulties in mass production.

Small size, simple design and an all-fiber configuration with high measurement accuracy are major requirements for fiber based electric field sensors. A polarimetric sensing scheme with

selectively LC infiltrated polarization maintaining PCF was demonstrated by the authors for electric field sensing [13]. The directional electric field sensitivity of the LC infiltrated PCF probe was also demonstrated by the authors [14]. In this paper we demonstrate for the first time the operation of an all-fiber electric field sensor based on a nematic liquid crystal (NLC) infiltrated solid core PCF which can be used in both end-point type and in-line type sensor configurations. The active region of the sensor probe, as demonstrated here, is a less than 1 cm long nematic liquid crystal infiltrated section of a commercially available solid core photonic crystal fiber. The sensor can be operated in transmission mode as an in-line sensor but also in reflection mode allowing for the implementation of an end point sensor. Since the birefringence of the infiltrated fiber is susceptible to variations in an external electric field, the sensing mechanism is intrinsic to this type of structure. The lateral size of the sensor is ~ 125 microns which is the cladding diameter of the PCF, and therefore the sensing device is intrinsically very compact, lightweight and can be easily integrated with fiber optics. The sensor operates in the telecommunications window at an operating wavelength of 1550 nm. The transmission and reflection response with electric field intensity is studied at 1550 nm and is presented here. Both the transmitted and reflected power of the infiltrated PCF shows a linear response with changing electric field intensity. Due to the temperature dependence of the infiltrated nematic LC mixture, the performance of the device is prone to temperature variations, therefore the temperature dependence of the sensor is also studied here for a temperature range from 10°C to 90°C.

2. Theoretical Background:

Solid silica core PCFs usually transmit light through a modified total internal reflection (m-TIR) mechanism. Infiltration of high-index materials (> n_{silica}) such as liquid crystals causes the transmission mechanism to change from m-TIR to photonic bandgap guidance. On infiltration the

holey cladding region of the PCF assumes the effective refractive index of the infiltrated LC material which is usually higher than that of the silica core region. Under these conditions the guiding properties of the PCF are primarily governed by the antiresonant reflection from multiple cladding layers and the transmission spectrum of the structure is determined by the refractive index contrast of the cladding layers [15].

When the nematic LC infiltrated cladding region of the PCF is subjected to an electric field, the NLC molecules undergo reorientation which changes the effective refractive index of the cladding and allows for tuning of photonic bandgap transmission. For LC mixtures which create planar alignment within the holes of the PCF, the propagation through the PCF core is governed by the ordinary refractive index of the infiltrated NLC, in the absence of external field.

On the application of an electric field above the threshold referred to as the Frederiks transition threshold [16] the LC molecules undergo reorientation within the micro holes. In the case of a liquid crystal layer of thickness d, the threshold electric field E_{th} for the LC reorientation is given as, $E_{th} \approx (\pi/d)\ (K_{11}(\varepsilon_{\shortparallel} - \varepsilon_{\perp}))^{1/2}$, where K_{11} is the splay elastic constant for the nematic LC and $\varepsilon_{\shortparallel}$, $\varepsilon_{\perp}$ are the dielectric permittivities [17]. As a simple approximation and assuming planar anchoring conditions, the hole diameter of the PCF can be treated as the effective thickness of the LC layer with a planar geometry.

Below the threshold field the propagation properties of the structure are governed by the ordinary refractive index of the LC given the long range orientation order of the LC molecules, aligned along the axis of the fiber (figure 1(a)). Above the threshold the LC molecules reorient themselves along the direction of the applied field and the propagation is governed by the effective refractive index, which is partially set by the extraordinary refractive index of the NLC. As the LC molecules begin to reorient under the action of the electric field, there is a loss in the uniformity of long range LC molecular alignment. With an increase in the applied electric field intensity, the formation of reverse tilted domains takes place which causes a loss in the LC long range orientation order. As a result the photonic bandgap condition for transmission in the

operating wavelength range is disturbed as light is coupled into the cladding region. In effect there is a gradual decrease in the power transmitted through the core of the LC infiltrated PCF with an increase in the electric field intensity.

3. Experimental Details:

A. E-field sensor probe:

The sensor probe fabricated for this demonstration is a < 1 cm long MDA-05-2782 infiltrated section of LMA-8 PCF, as shown in the figure 1(b). LMA-8 (figure 1(c)) is a commercially available circular core PCF designed for endlessly single mode operation with a core diameter of ~ 8.5 microns surrounded by seven rings of air-holes of 2.7 microns diameter arranged in a triangular lattice. The LC material MDA-05-2782 (Merck) is a nematic LC mixture. It has a clearing point at 106°C and its ordinary and extraordinary refractive indices are ~ 1.49 and ~ 1.61 correspondingly measured at 589.3 nm (Merck Datasheet).

To ensure effective core-to-core light coupling from SMF input fiber to PCF, a section of the PCF is spliced with a SMF-28 fiber using a standard fusion splicer [18]. The splicing conditions are optimized in order to ensure minimal air-hole collapse at the splice joint and also to provide sufficient mechanical strength for manual fiber handling. This is achieved by optimising the fusion current, fusion time and the number of re-arcs applied during the splicing. The coupling loss estimated after splicing was less than 2 dB for LMA-8 with SMF-28 fiber. The spectral response of the PCF in the wavelength range from 1500 to 1600 nm showed no interference pattern formation after splicing, which suggests that the splicing had not altered the endlessly single mode operation of LMA-8.

The open end of the PCF was infiltrated with MDA-05-2782 at room temperature by dipping the cleaved end into the LC material. The LC material was drawn into the PCF holes by capillary

action and an infiltration length of ~ 0.5 cm was obtained. The infiltrated end of the PCF was observed under a polarising microscope to examine the quality of infiltration and alignment. The broadband transmission spectrum of the infiltrated PCF sample was recorded using a tungsten halogen source and OSA. Figure 2, shows the recorded transmission spectrum of the infiltrated PCF in the wavelength range from 600 nm to 1700 nm. The low transmission region is observed to be in the wavelength range from 875 nm – 1150 nm. The structure has a photonic bandgap transmission region in the telecommunications wavelength window. An insertion loss of < 3 dB is estimated for the NLC infiltrated PCF at 1550 nm. The reflected spectrum recorded in the wavelength range from 1500 to 1600 nm was found to be flat and the formation of interference patterns was not observed.

B. E-field Measurement Principle and Experimental Arrangement:

The electric field is applied to the infiltrated PCF by means of two electrodes positioned on diametrically opposite sides of the cladding at the infiltrated end of the PCF. In order to avoid any movement or shaking of the fiber on the application of electric field due to electrostriction effect, the infiltrated end within the electrodes is firmly glued to the electrode surfaces. The distance between the electrodes is equal to the cladding diameter of the PCF which is 125 microns. In this geometry the electric field is applied perpendicularly to the fiber axis. As mentioned above, the infiltrated PCF sample displays high transmittance over a broad range of wavelengths. The application of the external electric field above the threshold value causes decrease in the transmittance which could be used for measurement of the electric field intensity. The electric field is applied to the infiltrated PCF using a combination of a high voltage power supply modulated by a standard waveform generator. This provides a positive polarity voltage waveform that varies in time in a sinusoidal fashion from zero volts up to a peak value, Vpeak, with an average value of Vpeak/2. The maximum value of Vpeak used in the experiment is 1200 V. The

frequencies used are 1 kHz and 50 Hz. A common practice in defining electric field intensity is to define it as volts-RMS per mm. Given the sinusoidal nature of the waveform the relationship between the Vpeak value and the RMS value is given by $Vrms = (3/8)^{1/2} Vpeak$. Therefore given the maximum value of Vpeak utilised, in effect the sensing device is subjected to an electric field intensity in the range from 0 to 6.0 kVrms/mm, given that the distance between the electrodes is ~ 125 microns. The experimental set-up to study the influence of electric field on the transmission properties and temperature dependence of the MDA-05-2782 infiltrated LMA-8 is shown in figure 3.

In our experiment linearly polarized light from a tunable laser source operating at a single wavelength of 1550 nm is coupled to the spliced PCF through a polarization controller to eliminate polarization induced instabilities. The output from the infiltrated end of the PCF is coupled to another SMF fiber by butt-coupling using a XYZ nano-positioner stage and is connected to a high speed optical power meter to record the transmittance as the applied electric field is varied. To study the infiltrated PCF sample in reflection mode the experimental setup as shown in figure 4 is employed. The light from the tunable laser source is passed through a fiber circulator and is coupled to the infiltrated PCF. In this case the infiltrated end of the PCF is left open and the reflected light from the air-PCF interface is coupled to a high speed optical powermeter for detection and measurement through the circulator.

4. Results and Discussion

A. Electric Field Intensity Measurements

A.1 Transmission response with electric field:

In this investigation a polarization controller is used to allow one to maximise the extinction ratio of the transmitted power at a high electric field when the infiltrated PCF becomes highly

birefringent. The measurement of transmission response is performed with the state of input polarization maintained in order to maximise the transmission extinction ratio and to improve the sensitivity of the device to an electric field. The transmission response of the device with increasing electric field intensity is shown in figure 5. Between a field intensity of zero and circa 2.35 kVrms/mm, the transmission response remains unchanged. Above this threshold field intensity, the NLC molecules begin to reorientate which results in a gradual decrease in transmission through the infiltrated PCF with the increasing electric field until an electric field intensity of ~ 4.89 kVrms/mm is reached. The transmission response in the range of electric field intensities from 2.35 kVrms/mm to 4.89 kVrms/mm is close to linear. The linear part of the transmission response for the infiltrated PCF in this electric field range is shown in figure 6. A linear fit performed for this electric field range shows that the slope of the response is ~ 10.1 dB-kVrms/mm confirming that MDA-05-2782 infiltrated LMA-8 can be used for electric field intensity measurements in this electric field range. Assuming an accuracy of 0.01 dB for the optical power measurement system, the estimated resolution of the device over the usable e-field intensity measurement range is ~ 1.0 kVrms/mm.

Given that one of the most likely applications of the sensor could be in a 50 Hz/60 Hz AC high voltage transmission environment, the device was also tested in the transmission mode for its sensitivity to a sinusoidally varying electric field at 50 Hz. The transmission response is as shown in figure 7. At 50 Hz a higher threshold electric field is observed (~ 2.93 kVrms/mm). Due to the limitations posed by the high voltage power supply in delivering peak voltages above 1200 V, it was not possible to extract the full linear range of the device with an applied 50 Hz AC voltage. However the transmission response in figure 6 confirms that the sensor can be used for 50 Hz/60 Hz AC voltage and electric field sensing.

The performance and sensitivity of the device can be further enhanced by employing the sensor in a ratiometric power measurement scheme. The threshold effect of the infiltrated LC puts a limit on the lower measurable electric field intensity. Since the threshold field is inversely proportional

to the hole diameter of the PCF, the use of a solid core PCF with larger hole diameter could reduce the threshold field for the device. Another viable solution for this could be the use of nematic LC mixtures which show a splayed alignment within the holes of the PCF [5]. Such LC mixtures do not show threshold effects and allow for continuous birefringence tuning of the infiltrated PCF from e-field intensities close to zero. Studies in this regard are in progress and will be the subject for a future publication.

A.2 Reflection response with electric field:

The reflected power response at 1550 nm with an increasing electric field (1 kHz) is as shown in figure 8. The reflected power from the infiltrated PCF end interface is relatively low (~ 20 dB), due to the low reflectance from the air-silica interface (~ 4%). The response with a varying electric field is found to be similar to that of the transmission response for the infiltrated PCF. Due to the expected low reflectance from the open PCF end the measured optical power was lower, leading to greater uncertainty in the measured values due to system noise. It should be noted that the use of the polarization controller in the reflection mode resulted in no change in the reflected power due the fact that the level of polarization maintenance in the reflection mode configuration is significantly lower than that in the transmission mode. Above the threshold field the reflected power decreases with an increasing electric field and the response is again found to be linear with the changing electric field. The linear sensing range is from ~ 2.35 kVrms/mm to ~5.14 kVrms/mm. The linearity of the reflected power with increasing electric field is depicted in figure 9, shown with the linear fit. The linear fit for the plot provides an estimate of the sensitivity of the device in reflection mode as ~ 4.55 dB-mm/kVrms. Assuming an accuracy of 0.01 dB for the optical detector in the measurement system, the estimated resolution of the device operated in the reflection mode is ~ 2.2 Vrms/mm. The reduced sensitivity of the device in the reflection mode is due to the fact that unpolarized light is used and that the state of polarization is not maintained after reflection from the open ended PCF. In a reflective type configuration the

infiltrated PCF can be used as an end point e-field sensor, which is an added advantage for the fabrication of sensors for e-field measurements in confined spaces.

Table 1 below lists the e-field sensing parameters estimated for MDA-05-2782 infiltrated LMA 8 PCF in both transmitted and reflection modes. As expected the sensitivity of the device as a sensor for e-field intensity is higher in the case with the transmission mode. It is possible to increase reflected power using a reflective coating at the open end of the PCF, improving the sensitivity of the device in the reflection mode.

B. Temperature Dependence of NLC Infiltrated PCF:

It is well known that temperature dependence of the transmission properties of PCF is minimal. However, the LC material used for infiltration has a temperature dependent refractive index [19]. The temperature dependence of the infiltrated PCF was studied at the operating wavelength of 1550 nm in order to evaluate the effect of temperature on the device performance and sensitivity. The infiltrated section of the fiber is kept at different temperatures using a Peltier module in the range from 10°C to 90°C and the electric field is varied. The transmission plots at different temperatures as obtained with change in electric field intensity in the range from 0 – 6 kVrms/mm are shown in figure 10. Figure 11 shows the plot as obtained for the reflection mode. As can be observed from the plots the sensor maintains its linear response in the electric field range from 2.35 kVrms/mm to 5.14 kVrms/mm. To evaluate the change in the sensitivity of the sensor with changes in temperature a linear fit was performed on the individual plots at each temperature for both the transmission and reflection modes in the linear electric field range from 2.35 kVrms/mm to 5.14 kVrms/mm. Figure 12 shows the sensitivity variation for the sensor in both reflection and transmission modes at different temperatures in the range from 10°C to 90°C.

The refractive indices (both n_e & n_o) of the liquid crystal decrease with an increase in temperature up to the NLC isotropic temperature (clearing point), resulting in a decrease of the effective refractive index of the cladding. In the temperature range from 10°C to 40°C it can be observed

that the change in the sensitivity is minimal, suggesting that the operation of the sensor is not influenced by temperature fluctuations in a range close to room temperature. At temperatures above the 40°C the slope, of the transmission plots with increasing electric field intensity, reduces and therefore the sensor sensitivity reduces for both operating modes. This is due to the fact that the effective refractive index of the cladding decreases at a lower rate with temperature for a temperature range from 10 °C to 40 °C, while above 40 °C the rate of decrease increases as the temperature approaches the clearing point (106 °C) of the NLC material used.

For the measurement of e-fields at room temperature, the sensor is influenced minimally by temperature change. For the temperature range from 40°C and up to 90°C there is significant change in the sensitivity of the sensor in both the transmitted mode and reflected mode but the response (transmitted & reflected) of the sensor maintains it's linearity in the measurable electric field range. To maintain accuracy across a broader range of operating temperatures, the sensor would need an associated means of temperature monitoring and correction.

5. Conclusions:

The application of nematic LC infiltrated solid core photonic crystal fiber as an all-fiber based electric field intensity measurement device is demonstrated. The sensor, based on the electronic tunability of the infiltrated PCF, has a linear transmission and reflection response with changing electric field intensity. The sensor probe consists of less than 1 cm long infiltrated section of a solid core photonic crystal fiber and has a lateral size of ~ 125 microns. A simple all-fiber design for the sensor makes it compact and allows for easy integration and coupling with fiber optics. A light intensity based measurement scheme is employed with the sensor operating in the telecommunications window at 1550 nm. With the proper choice of PCF and liquid crystal, the sensor can be designed to work in a desired measurable electric field range with improved sensitivity. The device is capable of operating as an in-line sensor in the transmitted mode and also as an end point sensor in the reflected mode. The temperature dependence of the sensor

probe at an operating wavelength of 1550 nm has been studied and the sensor is shown to have a moderate temperature sensitivity for a room temperature environment. For a high temperature environment as in the case of the measurement of electric fields at high power electrical facilities and high voltage transmission lines, the device can be operated with correction for temperature which would require addition of a temperature monitor. As an inherent electric field sensing devices these devices can also be used for high voltage sensing with the voltage being applied using a fixed electrode configuration.

6. References:

1. T. Larsen, A. Bjarklev, D. Hermann, and J. Broeng, "Optical devices based on liquid crystal photonic bandgap fibres," Opt. Exp. 11, 2589-2596 (2003).
2. D. Noordegraaf, L. Scolari, J. Lægsgaard, L. Rindorf, T. T. Alkeskjold, "Electrically and mechanically induced long period gratings in liquid crystal photonic bandgap fibers", Opt. Exp., 15, 7901-7912 (2007).
3. T.T. Alkeskjold, L. Scolari, D. Noordegraaf, J. Lægsgaard, J. Weirich, L. Wei, G. Tartarini, P. Bassi, S. Gauza, S. T. Wu, and A. Bjarklev, "Integrating liquid crystal based optical devices in photonic crystal fibers," Opt. Quant. Electron. 39, 1009-1019 (2007).
4. T.R. Wolinski, K. Szaniawska, S. Ertman, P. Lesiak, A.W. Domanski, R. Dabrowski, E.N. Kruszelnicki, and J. Wojcik, "Influence of temperature and electric fields on propagation properties of photonic liquid crystal fibers," Meas. Sci. Tech. 17, 985-991 (2006).
5. L. Scolari, T.T. Alkeskjold, J. Riishede, A. Bjarklev, "Continuosly tunable devices based on electrical control of dual-frequency liquid crystal filled photonic bandgap fibers," Opt. Exp. 13, 7483-7496 (2005).
6. S. Mathews, Y. Semenova, and G. Farrell, "Electronic tunability of ferroelectric liquid crystal infiltrated photonic crystal fiber," Electron. Lett. 45, 617-618 (2009).

7. V.M.N. Passaro, F. Dell'Olio, and F. De Leonardis, "Electromagnetic field photonic sensors," Prog. Quant. Elect. 30, 45-73 (2006).
8. C.G. Martinez, J.S. Aguilar, and R.O. Valiente, "An all-fiber and integrated optics electric field sensing scheme using matched optical delays and coherence modulation of light," Meas. Sci. Technol. 15, 3223-3229 (2007).
9. H. Togo, N. Kukutsu, N. Shimizu, and T. Nagatsuma, "Sensitivity-stabilized fiber-mounted electrooptic probe for electric field mapping," J. Lightwave. Technol. 26, 2700-2705 (2008).
10. M. Bernier, G. Gaborit, L. Du Villaret, A. Paupet, and J.L. Lasserre, "Electric field and temperature measurement using ultra wide bandwidth pigtailed electro-optic probes," App. Opt. 47, 2470-2476 (2008).
11. C. Li, and T. Yoshino, "Optical voltage sensor based on electrooptic crystal multiplier," J. Lightwave. Technol. 20, 843-849 (2002).
12. A. Michie, I. Bassett, J. Haywood, "Electric field and voltage sensing using thermally poled silica fibre with a simple low coherence interferometer," Meas. Sci. Technol. 17, 1229-1233 (2006).
13. S. Mathews, G. Farrell, and Y. Semenova, "All-fiber polarimetric electric field sensing using liquid crystal infiltrated photonic crystal fibers," Sens & Act A: Physical, In Press, Jan 2011.
14. S. Mathews, G. Farrell, and Y. Semenova, "Directional electric field sensitivity of liquid crystal infiltrated photonic crystal fiber," Photon. Technol. Lett. 23, 408-410 (2011).
15. N.M. Litchinitser, A.K. Abeeluck, C. Headley, and B.J. Eggleton, "Antiresonating reflecting photonic crystal optical waveguides," Opt. Lett. 27, 1592-1594 (2002).
16. M.W. Haakestad, T.T. Alkeskjold, M.D. Nielsen, L. Scolari, J. Riishede, H.E. Engan, and A. Bjarklev, "Electrically tunable photonic bandgap guidance in a liquid crystal filled photonic crystal fiber," Photon. Technol. Lett. 17, 819-821 (2005).
17. D. Demus, J. Gooby, G. W. Gray, H.W. Spiess, and V. Vill, Physical properties of liquid crystals, (Wiley-VCH, 1999).

18. L. Xiao, M.S. Demokan, W. Jin, Y. Wang, and C. Zhao, “Fusion splicing photonic crystal fibers and conventional single-mode fibers: microhole collapse effect,” J. Lightwave. Technol. 25, 3563- 3574 (2007).

19. J. Li, S. Gauza, and S. T. Wu, “Temperature effect on liquid crystal refractive indices”, J. App. Phy., 96, 19-24 (2004).

Figures:

Figure 1:

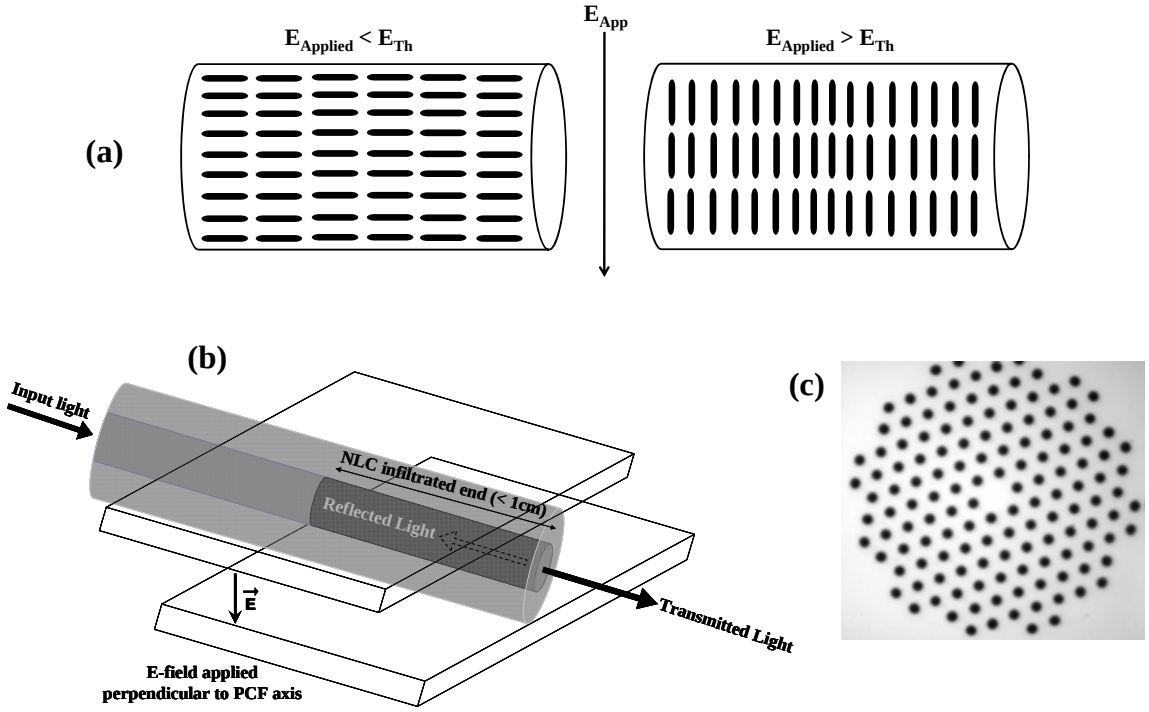

Figure 2:

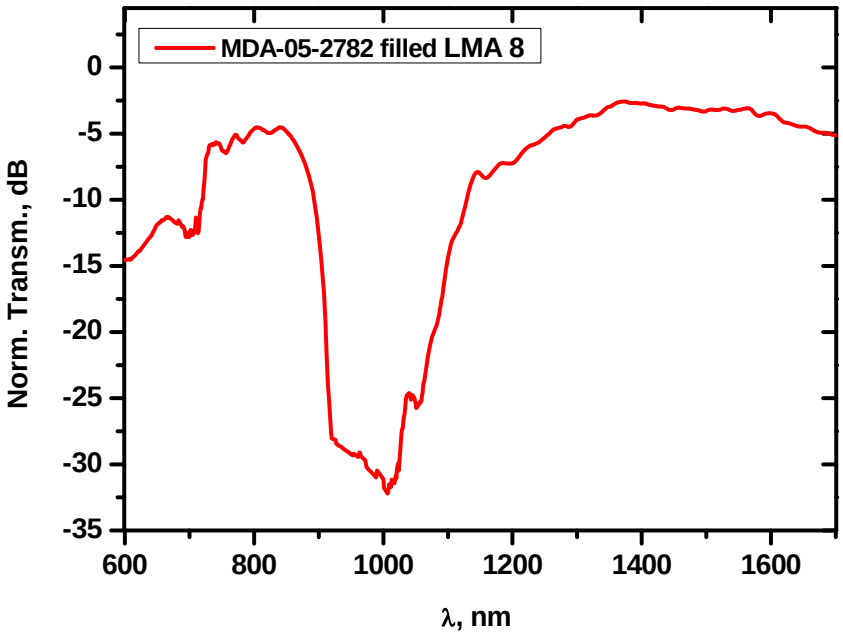
MDA-05-2782 filled LMA 8
Norm. Transm., dB
0
-5
-10
-15
-20
-25
-30
-35
600
800
1000
1200
1400
1600
λ, nm

Figure 3:

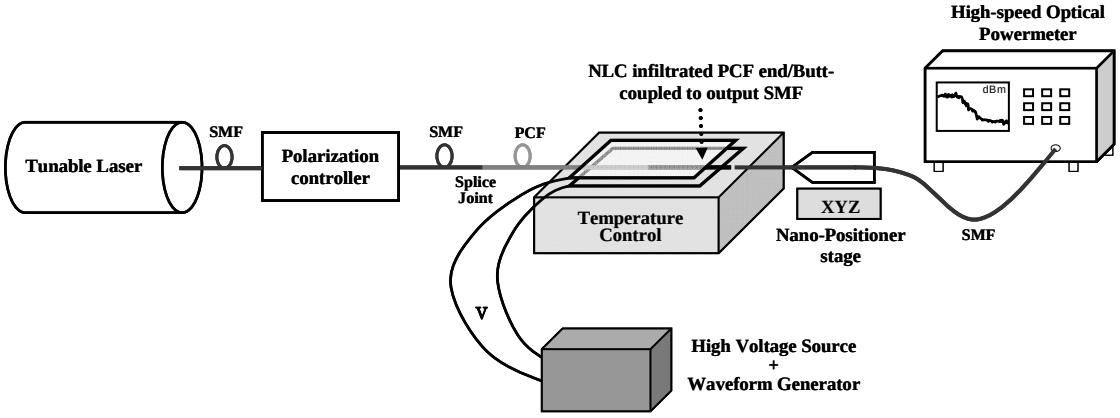
High-speed Optical Powermeter
NLC infiltrated PCF end/Butt-coupled to output SMF
dBm
Tunable Laser
SMF
Polarization controller
SMF
PCF
Splice Joint
Temperature Control
XYZ
Nano-Positioner stage
SMF
V
High Voltage Source
+
Waveform Generator

Figure 4:

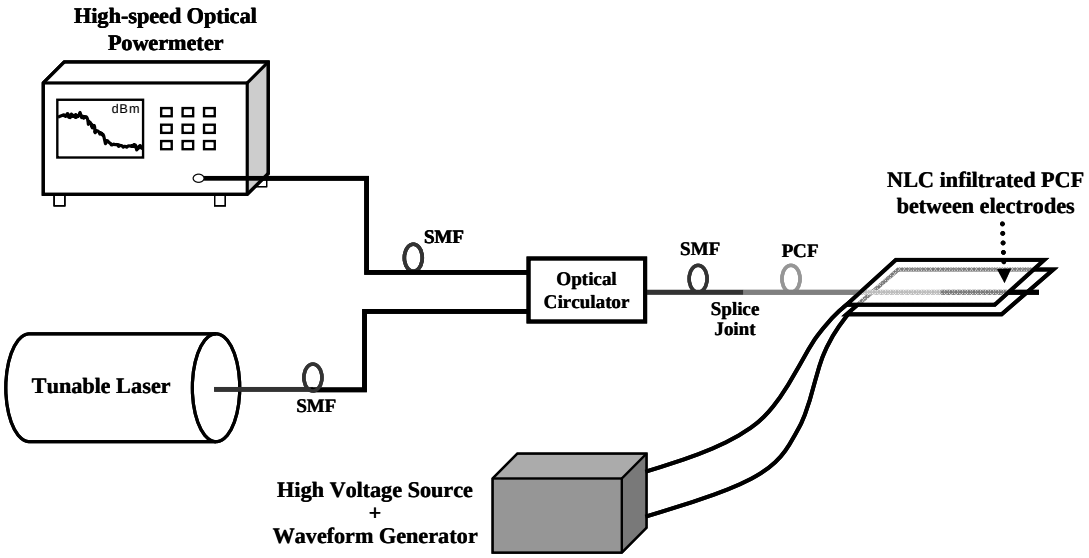
High-speed Optical Powermeter
dBm
SMF
Optical Circulator
SMF
PCF
NLC infiltrated PCF between electrodes
Splice Joint
Tunable Laser
SMF
High Voltage Source + Waveform Generator

Figure 5:

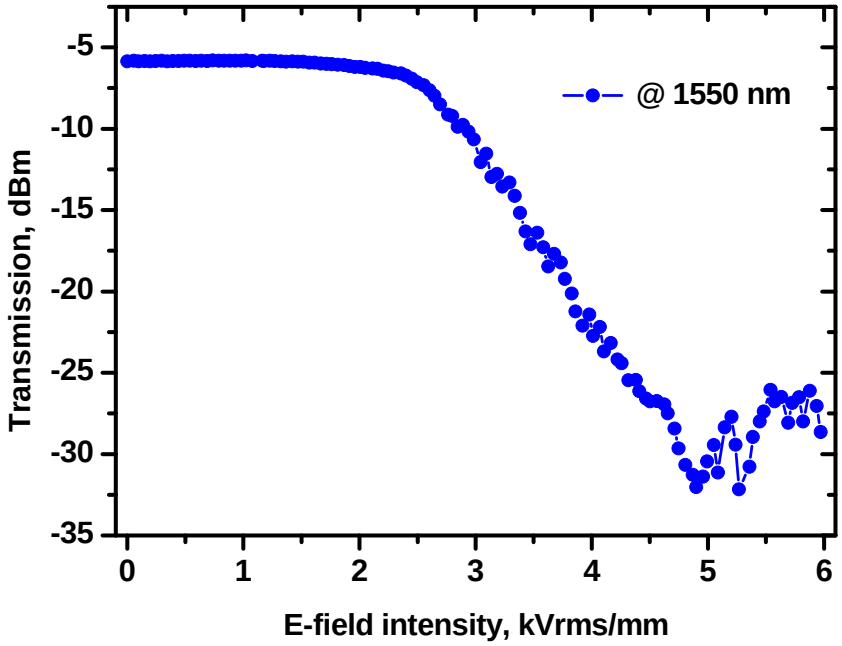
Transmission, dBm
-5
-10
-15
-20
-25
-30
-35
0
1
2
3
4
5
6
E-field intensity, kVrms/mm
@ 1550 nm

Figure 6:

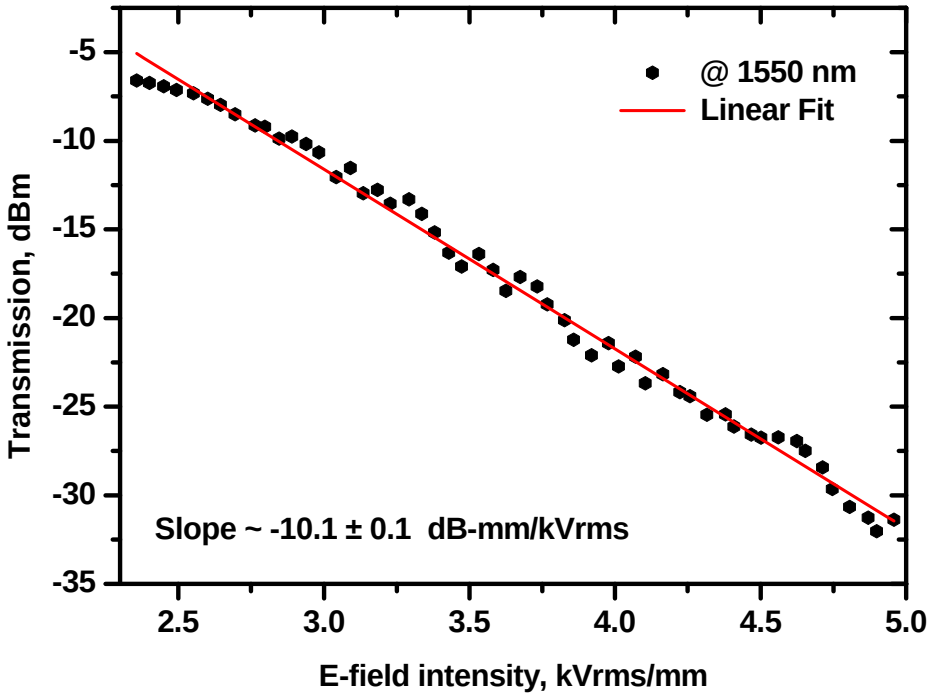
@ 1550 nm
Linear Fit
Slope ~ -10.1 ± 0.1 dB-mm/kVrms
Transmission, dBm
E-field intensity, kVrms/mm
-5
-10
-15
-20
-25
-30
-35
2.5
3.0
3.5
4.0
4.5
5.0

Figure 7:

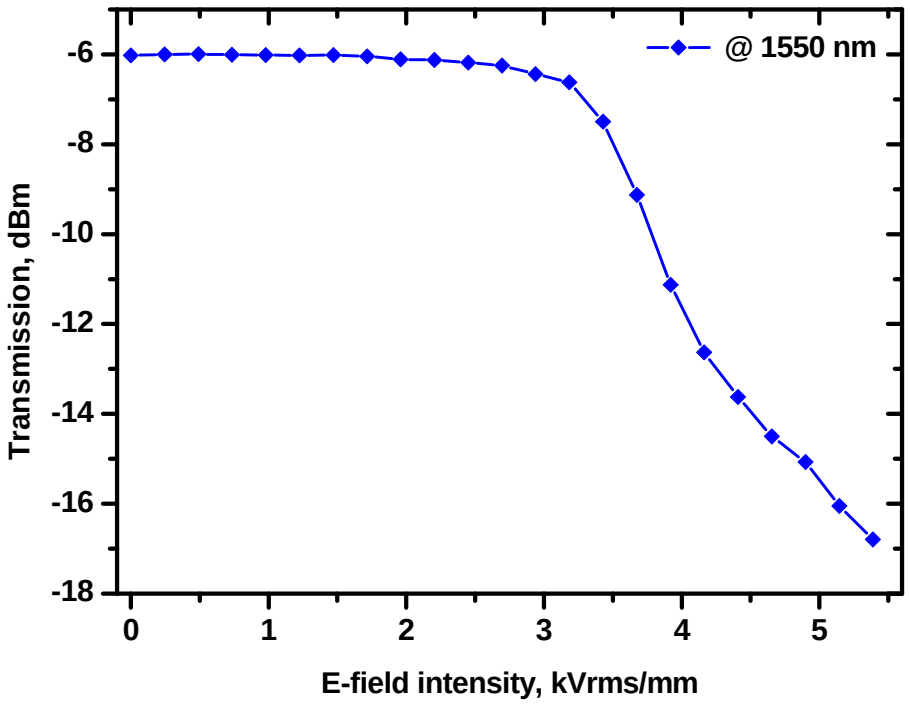
@ 1550 nm
Transmission, dBm
-6
-8
-10
-12
-14
-16
-18
0
1
2
3
4
5
E-field intensity, kVrms/mm

Figure 8:

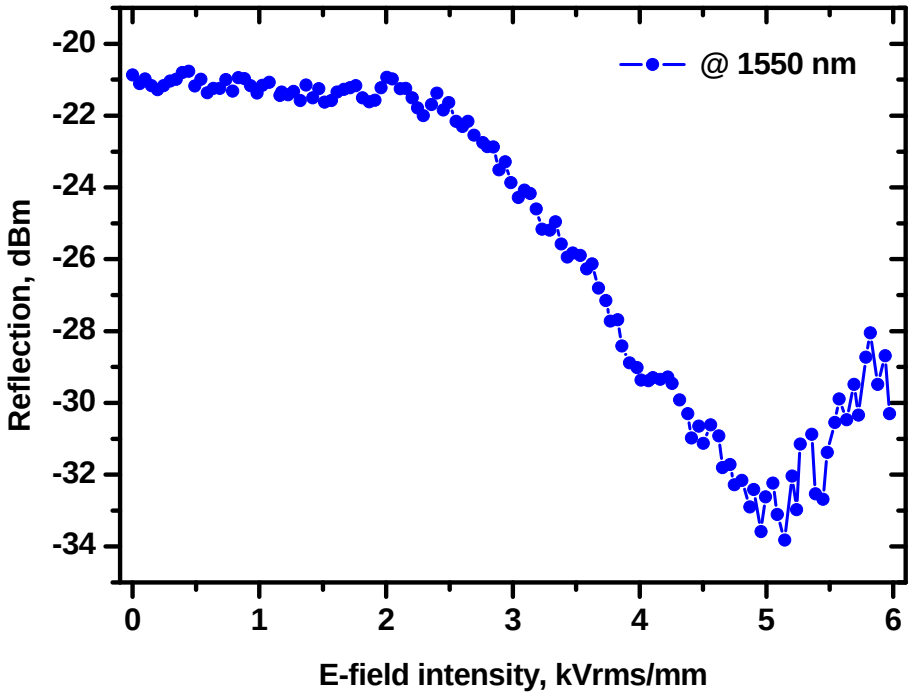
@ 1550 nm
Reflection, dBm
-20
-22
-24
-26
-28
-30
-32
-34
0
1
2
3
4
5
6
E-field intensity, kVrms/mm

Figure 9:

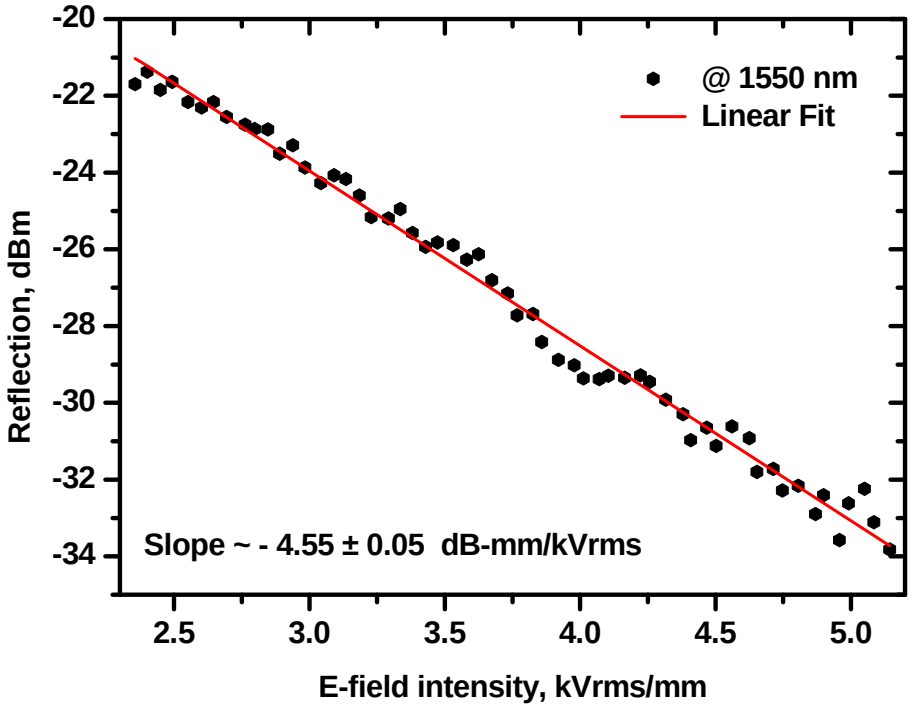
-20
-22
-24
-26
-28
-30
-32
-34
Reflection, dBm
2.5
3.0
3.5
4.0
4.5
5.0
E-field intensity, kVrms/mm
@ 1550 nm
Linear Fit
Slope ~ - 4.55 ± 0.05 dB-mm/kVrms

Figure 10:

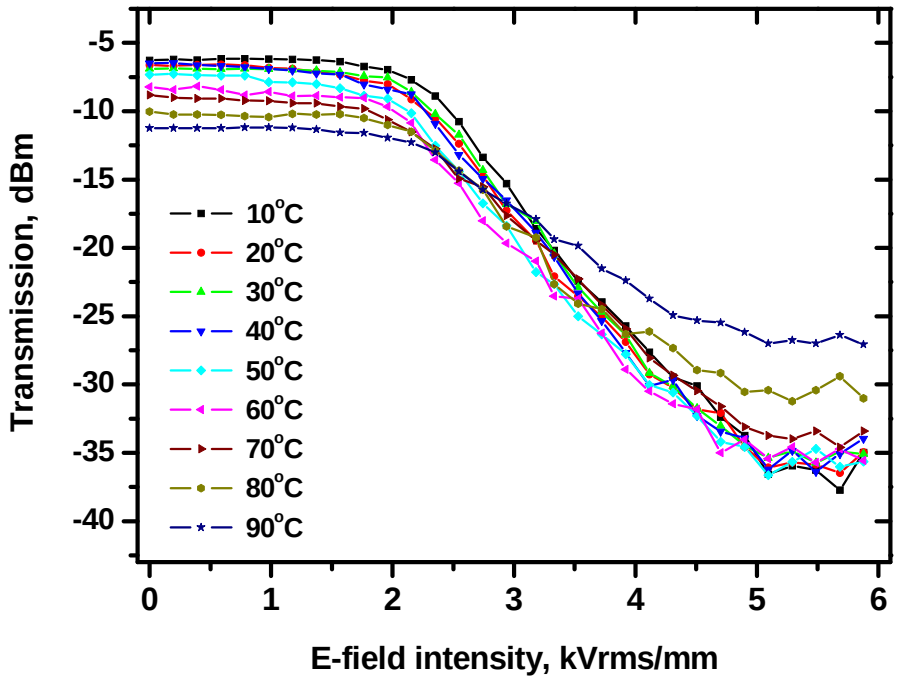
Transmission, dBm
-5
-10
-15
-20
-25
-30
-35
-40
0
1
2
3
4
5
6
E-field intensity, kVrms/mm
10°C
20°C
30°C
40°C
50°C
60°C
70°C
80°C
90°C

Figure 11:

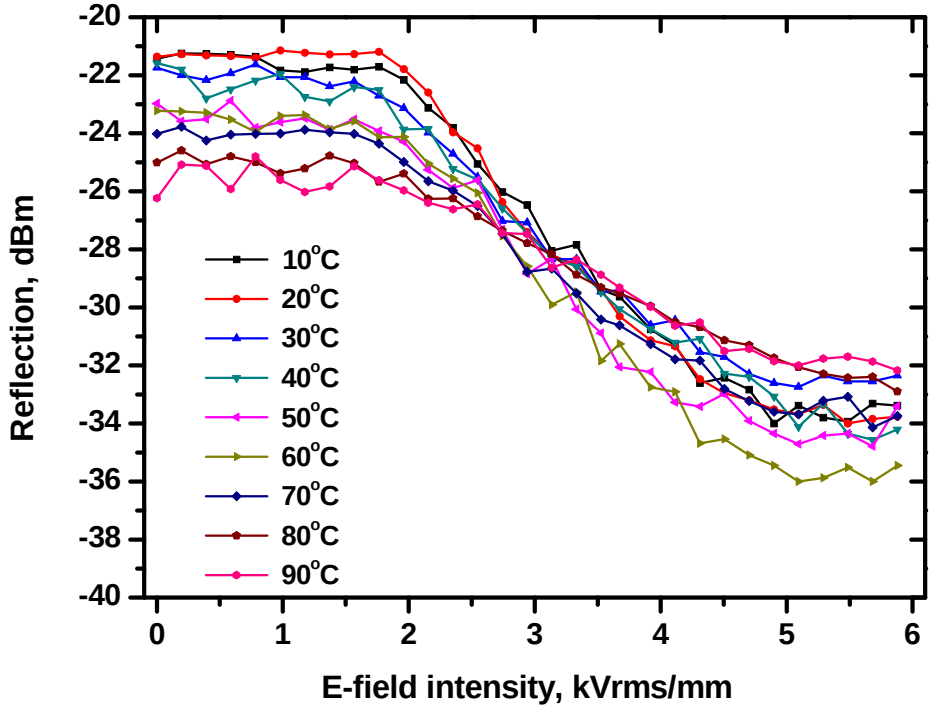
Reflection, dBm
E-field intensity, kVrms/mm
-20
-22
-24
-26
-28
-30
-32
-34
-36
-38
-40
0
1
2
3
4
5
6
10°C
20°C
30°C
40°C
50°C
60°C
70°C
80°C
90°C

Figure 12:

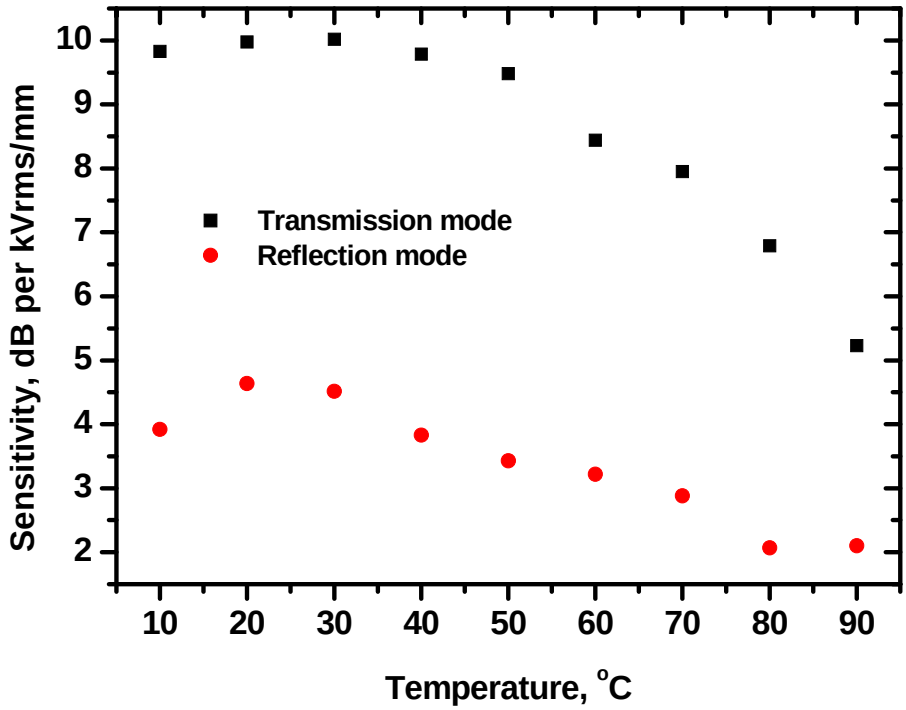
Sensitivity, dB per kVrms/mm
Temperature, °C
Transmission mode
Reflection mode
10
9
8
7
6
5
4
3
2
10
20
30
40
50
60
70
80
90

Figure Captions:

Fig 1: (a) Orientation of LC molecules within PCF holes below and above the threshold field, (b) Nematic LC infiltrated PCF probe for electric field sensing within electrodes, and (c) SEM image of LMA-8 cross-section (Fiber specs sheet; NKT Photonics).

Fig 2: Broadband transmission spectrum (600 nm – 1700 nm) of MDA-50-2782 infiltrated LMA-8 PCF.

Fig 3: Schematic of the experimental setup to study the electronic tunability and temperature dependence of the NLC infiltrated PCF.

Fig 4: Schematic of the experimental setup to study reflected power response of the infiltrated PCF.

Fig 5: Transmission response of MDA-05-2782 infiltrated LMA-8 with a changing electric field intensity (1 kHz) at 1550 nm measured at room temperature.

Fig 6: Linear part of the transmission response of MDA-05-2782 infiltrated LMA-8 with electric field intensity (1 kHz) at 1550 nm shown with a linear fit.

Fig 7: The transmission response of MDA-05-2782 infiltrated LMA-8 with electric field intensity (50 Hz) at 1550 nm measured at room temperature.

Fig 8: Reflected power response of MDA-05-2782 infiltrated LMA-8 with a changing electric field intensity (1 kHz) at 1550 nm measured at room temperature.

Fig 9: Linear part of the reflected power response of MDA-05-2782 infiltrated LMA-8 with electric field intensity (1 kHz) at 1550 nm shown with a linear fit.

Fig 10: Transmission response of the sensor versus electric field intensity at different temperatures from 10°C to 90°C.

Fig 11: Reflection response of the sensor versus electric field intensity at different temperatures from 10°C to 90°C.

Fig 12: E-field sensitivity variation with temperature change for transmission and reflection modes.

Tables:

Table 1: Comparison of e-field sensing parameters of MDA-05-2782 infiltrated LMA-8 in different modes.

Sensor configuration	Sensitivity (dB per kVrms/mm)	Measurable e-field intensity range (kVrms/mm)	Estimated Resolution (Vrms/mm)
Transmitted mode (In-line type)	~ 10.1	2.35 – 4.95	~ 1
Reflected mode (end-point type)	~ 4.55	2.35 – 5.14	~ 2.2